Water storage in cratonic mantle

Emily J. Chin[1*] and Richard M. Palin[2]

[1] *Scripps Institution of Oceanography, UC San Diego, La Jolla, CA 92093, USA*

[2] *Department of Earth Sciences, University of Oxford, South Parks Road, OX1 3AN, UK*

[*]Corresponding author: e8chin@ucsd.edu

ABSTRACT

Knowledge of the water capacity of deep lithosphere is crucial for validating models of craton growth and for constraining solid earth volatile cycles over geologic time. However, experimental constraints on water solubility and partitioning often disagree with natural rock data. We present a bulk compositionally dependent model of water storage capacity in pyrolite over a range of lithospheric mantle pressures and temperatures. Models are compared against published xenolith nominally anhydrous mineral (NAM) water contents, which have been recalculated to reflect the last water content of the mantle lithosphere by using coexisting pyroxene water contents in the same samples. Our main findings are that 1) regardless of tectonic setting, olivine records similar recalculated water contents, suggesting a common level of water undersaturation in the lithospheric mantle, and 2) equilibrium water partitioning between clinopyroxene and orthopyroxene (Dcpx/opx) increases down-temperature. We propose these trends may be explained by re-hydration/re-fertilization of cratonic mantle early during

coalescence, followed by cooling-induced water exsolution from orthopyroxene and garnet formation as cratons thicken and stabilize.

INTRODUCTION

Mantle water content is an important parameter that controls its petro-physical properties and, as a consequence, evolution of the mantle lithosphere over Earth's history. On the present-day Earth, distribution of water in the mantle varies across tectonic setting, with depleted upper mantle containing 50–200 parts per million (ppm) H_2O by weight (Demouchy and Bolfan-Casanova, 2016; Hirschmann, 2006), but up to 1500 ppm H_2O occurring above subducted, devolatilized oceanic slabs (e.g., Ulmer, 2001). These variations largely reflect processes that have shaped the Earth's mantle during the Phanerozoic, since "cold, steep, and deep" subduction became the dominant mechanism of volatile input into the deep Earth (Bodnar et al., 2013; Palin et al., 2020).

In contrast to Phanerozoic Earth, the geodynamics of early Earth are more enigmatic, but likely differed significantly from the style of plate tectonics that operates today (e.g. Piccolo et al., 2020). Higher initial mantle potential temperatures (e.g. Herzberg et al., 2010; Ganne and Feng, 2017) led to unique styles and compositions of magmatism, which infer that different mechanisms of lithospheric evolution governed the Archean and Proterozoic compared to the Phanerozoic (Condie, 2021). The influence of volatiles on mantle and crustal deformation and geodynamics may also have evolved during these regime shifts, as distributions of melt inclusions in high-grade rocks through geologic time show peaks correlating with major plate tectonic transitions (Nicoli and Ferrero, 2021). In addition, the water carrying capacity of altered oceanic crust is also

thought to have been higher in the geological past than today, owing to an evolution in its maficity (e.g. Palin and White, 2016).

The most significant tectonic development in early Earth history was the fusion of lithospheric nuclei into cratons, setting the stage for formation of the continents. However, the mechanisms by which cratons coalesced remains open to debate (Pearson et al., 2021). On one hand, cratons must have remained cold, thick, and buoyant for long periods of time to satisfy current seismic imaging, xenolith constraints, and heatflow data. On the other hand, at some point in the cratons' evolution, they must have been deformable enough to suture into large blocks, perhaps facilitated by hydrated mantle shear zones (Lee et al., 2008). Trace amounts of water in olivine enhances the creep rate via hydrolytic weakening (Brodholt and Refson, 2000) and water also lowers mantle viscosity (Hirth and Kohlstedt, 1996), with both factors enhancing deformation. Present-day constraints of water content in the cratonic mantle from xenoliths show spatial heterogeneity at both vertical and lateral scales (Peslier et al., 2017). However, the origins of such water heterogeneity are not agreed upon – either it was inherited, i.e. "frozen in" after the cratons formed, like fossil seismic anisotropy that somehow persists over billions of years (Silver and Chan, 1988), or, post-cratonization metasomatism modified the original hydration state of the cratonic mantle.

While metasomatized mantle may contain hydrous minerals, the vast majority of cratonic mantle is highly depleted (Lee et al., 2011), which confers the long-lived chemical buoyancy needed to counteract the negative buoyancy associated with a cold, thick thermal boundary layer (Jordan, 1981). The largest mantle water reservoir is incorporated within nominally anhydrous minerals (NAMs) (Bell and Rossman, 1992)

where water is substituted as various species in crystal lattice defects. Water solubility in NAMs increases with increasing pressure, and experimental mineral/melt partition coefficients are highest for clinopyroxene and orthopyroxene followed by garnet, then olivine (Aubaud et al., 2004; Hauri et al., 2006; Tenner et al., 2009). Here, the partition coefficient is defined as the ratio of the concentration of a trace element (in this case, water) in the mineral to that in the melt at equilibrium: $D_{mineral}^{H2O} = \frac{C_{mineral}^{H2O}}{C_{melt}^{H2O}}$.

Pyroxenes, in particular, are an important NAM water reservoir owing to them having higher D values compared to olivine and garnet. Hauri et al. (2006) found that D positively correlates with Al in orthopyroxene, owing to the coupled substitutions $H^+ + Al^{3+} \leftrightarrow 2\ Mg^{2+}$ and $H^+ + Al^{3+} \leftrightarrow Si^{4+}$ (Keppler and Bolfan-Casanova, 2006). Aluminum-free enstatite has comparable H-solubility to clinopyroxene at <4.5 GPa, but Al-bearing enstatite may contain up to three times as much H_2O at these conditions (Mierdel et al., 2007). Importantly, $D_{Cpx/Opx}$, converges to values ~1 for melt-present, high-T conditions (>1000 °C) (Hauri et al., 2006), though subsolidus values are higher at ~2 (Demouchy et al., 2017). This suggests that water partitions equally between clinopyroxene and orthopyroxene in the presence of partial melt, but water is preferentially partitioned into clinopyroxene as the mantle cools.

Despite extensive experimental and observational data on water partitioning between mantle NAMs, straightforward interpretation of measured NAM water contents in exhumed mantle rocks remains challenging. This is largely due to: (1) a lack of synergistic information reported from xenoliths (e.g. the absence of calculated final equilibration *P–T* conditions that constrain the sample's thermal history); (2) H^+ only measured in one NAM, but not in coexisting minerals, thus prohibiting effective

93 determination of partitioning relationships; and (3) the lack of a thermodynamically
94 based framework for predicting the maximum solubility of H^+ in different NAMs as a
95 function of *P*, *T*, and mineral composition. While individual parameterizations exist for
96 certain NAMs, as derived from high-*P*/high-*T* laboratory experiments, an integrated
97 approach is needed that considers all coexisting NAMs within mantle rocks to
98 quantitatively compare water storage model predictions as a function of geodynamic
99 environment to measured data obtained from natural peridotites. Here, we directly
100 address this issue, and combine a survey of global xenolith NAM water data with the
101 results of petrological forward modelling at upper mantle *P*–*T* conditions, which allows
102 us to determine mineral equilibria and storage capacities in canonical pyrolite mantle
103 (Ringwood, 1975) **(Fig. 1a)**. We then compare these predictions to H_2O contents from
104 mantle xenoliths erupted within cratonic and non-cratonic regions worldwide, and
105 propose that cooling-induced hydrogen loss (or "sweating") during craton formation is a
106 common geological phenomenon, which may be necessary for cratons' long-term
107 preservation.
108
109 **H_2O CAPACITY OF MANTLE NAMS**
110 **Models**
111 Stable phase equilibria for anhydrous pyrolite (Ringwood, 1975) and an average
112 garnet harzburgite from the Slave craton (Kopylova and Russell, 2000) **(Fig. S1)** were
113 calculated in the Na_2O–CaO–FeO–MgO–Al_2O_3–SiO_2–Cr_2O_3 (NCFMASCr) chemical
114 system using the Gibbs free energy minimization modeling program Theriak-Domino
115 (De Capitani and Petrakakis, 2010), internally consistent thermodynamic dataset ds-622

(Holland and Powell, 2011), and activity–composition relations for olivine, garnet, clinopyroxene, orthopyroxene, spinel, plagioclase, and ultramafic silicate melt (Jennings and Holland, 2015). The pyrolite and Slave compositions were selected as representative end members of typical cratonic mantle lithosphere. The Slave sample's lower Al_2O_3 content and slightly higher XMg **(Table S1)** expands the orthopyroxene stability field compared to pyrolite and suppresses garnet stability, but other phase relations are similar. Calculated phase relations for pyrolite **(SI Fig. 1a–b)** resemble those for typical peridotite (cf. KLB-1; Jennings and Holland, 2015).

The potential H_2O contents (ppm) of diopside, pyrope, Al-free enstatite, and olivine (Fo = 0.9) **(Fig. S3)** were individually calculated within the pressure–temperature (*P*–*T*) range 0–5 GPa and 600–1600 °C using parameterizations experimentally determined by Bromiley et al. (2004), Lu and Keppler (1997), Mierdel and Keppler (2004), and Zhao et al. (2004), respectively, alongside the Pitzer and Sterner (1994) equation of state for H_2O. For both considered bulk compositions, the total potential bulk H_2O content hosted within NAMs at any given *P*–*T* condition **(Fig. S3)** was determined using a two-step mass-balance procedure: (1) calculated volume proportions of each NAM were converted to weight percentages using their densities, and then individually combined with their maximum H_2O content at that *P*–*T* point; and (2) bulk rock H_2O content was calculated by summing the H_2O contents of each mineral constituent with respect to their individual mass fraction. Contributions from olivine in the bulk pyrolite model considered variations in the calculated equilibrium Fo content [atomic Mg/(Mg + Fe)] over the modeled *P*–*T* range.

The calculated potential H_2O content of individual NAMs is shown in **Fig. 1b-d**, and that for bulk pyrolite was determined from a weighted calculation involving the proportions of each phase and their individual H solubilities at *P*–*T* conditions relevant to continental lithospheric mantle. The potential H_2O carrying capacity increases with *P* and *T*, ranging from ~30–60 ppm at 600 °C and 1–3 GPa, and up to ~2400 ppm at 5 GPa at ~1400 °C **(Fig. 1a)**. H_2O carrying capacities in individual NAMs along model geotherms for cold, moderate, and warm cratonic lithosphere are shown in **Fig. 1b-d** and are compared to xenolith data in **Fig. 2 and Fig. 3**. Modeled mineral composition and phase proportion data within this *P*–*T* space and along specific geotherms are detailed in **Figs. S1–6**.

Xenolith data

Given the strong thermobarometric dependence of hydrogen solubility in NAMs, the tectonic and thermal evolution of a xenolith should be considered when interpreting lithospheric water content. Literature data (see **SI** for references) have been compiled for mantle xenoliths that report H_2O concentrations in coexisting olivine, orthopyroxene, and clinopyroxene and a previously published final *P*–*T* condition of equilibration (**SI Table 3**). As we discuss further in the following section, our filtering of published xenolith NAM H_2O values yields an internally consistent dataset, as we recalculate olivine H_2O contents using both orthopyroxene and clinopyroxene present in the same xenolith (discussed below). While this approach results in fewer plotted data points **(Fig. 2, 3)** compared to previous literature surveys of NAM H_2O in mantle minerals (Peslier, 2010;

Demouchy and Casanova, 2016; Peslier et al., 2017) it allows a direct comparison to experimentally derived H_2O partitioning studies as well as our phase equilibria models.

Calculated final *P*–*T* conditions for xenoliths from Siberia, Kaapvaal, and Wyoming Cratons plot close to geotherms corresponding to low heat flow (30–40 mW m^{-2}), which is characteristic of present-day Archean shields (e.g., Pollack and Chapman, 1977) **(Fig. 3a)**. A notable exception in this data set is the North China Craton, with xenoliths plotting along a hotter geotherm **(Fig. 3a)**, consistent with proposed recent magmatic rejuvenation and lithospheric thinning (Xu et al., 2009). Off-craton xenoliths from the Basin and Range, USA, which fall close to or above the 60 mW m^{-2} geotherm **(Fig. 3)**, also reflect actively extending lithosphere. Off-craton xenoliths from Mexico and Simcoe plot near to the 60 mW m^{-2} geotherm, which is typical of active arcs (e.g. Ziagos et al., 1985). In contrast, xenoliths sampling the extinct Sierra Nevada arc (subduction ended at ~80 Ma; garnet-bearing xenoliths were erupted at ~8 Ma) plot along a 40 mW m^{-2} geotherm, similar to cratons, and indicative of the cold and thick final conditions of the Sierran arc root (Chin et al., 2015).

Seeing through the "veil" of diffusive loss of water in NAMs

A major concern when studying volatiles in NAMs is the extent to which post-formation processes affect the water content of the mineral (i.e. determining whether the measured concentration is primary or secondary). For xenoliths, rapid diffusive water loss from olivine during ascent to the Earth's surface is common (Mackwell and Kohlstedt, 1990). Importantly, the activation energy for H^+ diffusivity in olivine is higher than that for pyroxenes (Xu et al., 2019). Thus, at high *T* (>1000 °C), diffusive

185 water loss may be significant in olivine, but negligible in pyroxene, despite similar
186 diffusivities at lower temperatures in both minerals.
187 Given the large difference in diffusivity at >1000 °C (Xu et al., 2019),
188 clinopyroxene water contents in erupted xenoliths may be less susceptible to water loss
189 compared to orthopyroxene and olivine (Warren and Hauri, 2014; Chin et al., 2021).
190 However, limited xenolith evidence also suggests that orthopyroxene may be more
191 susceptible to diffusive water loss compared to clinopyroxene (Tian et al., 2017). Thus,
192 we use the water contents of clinopyroxene, where available in the same xenoliths, to
193 recalculate olivine water contents to concentrations that were last in equilibrium with the
194 pyroxene, assuming that present-day water contents reflect some post-formation water
195 loss. We refer to these recalculated values, abbreviated as "RC" henceforth, as "last"
196 values, denoting the water content that was presumably reflective of last equilibration in
197 the lithosphere. We also recalculated olivine water contents based on water contents of
198 orthopyroxenes coexisting with olivine (see **SI Table 1**), but for the purposes of this
199 paper, focus on clinopyroxene-recalculated olivine water contents based on the
200 diffusivity arguments above.
201 To obtain RC olivine water contents from our compilation of observed olivine
202 water contents, we used an averaged experimental partition coefficient of $D_{cpx/ol} = 12$
203 from Hauri et al. (2006). In other words, RC C_{H2O} olivine = (measured C_{H2O} cpx)/12.
204 While $D_{pyroxene/H2O}$ varies as a function of the Al^{3+} content in pyroxene (Hauri et al.,
205 2006), this effect is most pronounced at high Al_2O_3 (>4 wt. %). Most cratonic pyroxenes,
206 particularly those that have equilibrated with garnet, have <4 wt. % Al_2O_3 (Pearson et al.,
207 2003). Unfortunately, there is a lack of experimental data on the variation of $D_{Pyroxene/H2O}$

208 for such low-Al^{3+} pyroxenes, and so we use a fixed ($D_{Cpx/Ol}$ = 12) partition coefficient in
209 all olivine water recalculation. **Figure 2** compares observed olivine water content with
210 recalculated-to-clinopyroxene olivine (RC) water content.
211 In their comprehensive survey of mantle peridotites, Warren and Hauri (2014)
212 found that both clino- and orthopyroxene water contents may be better archives of
213 primary mantle hydration state than olivine or either pyroxene alone. In particular, the
214 ratio of water contents in coexisting pyroxene pairs (R_{cpx}/R_{opx}) is often compared to
215 experimentally determined $D_{mineral/melt}$ values – from which an effective $D_{cpx/opx}$ can be
216 calculated – to assess the degree of equilibrium. For $R_{cpx/opx}$, Warren and Hauri (2014)
217 compiled literature xenolith data and report an equilibrium value of 2.6 ± 0.9 (n = 141).
218 By contrast, the average experimental $D_{cpx/opx}$ is 1.3 ± 0.3 (n = 10) (Aubaud et al., 2004;
219 Hauri et al., 2006; O'Leary et al., 2010; Tenner et al., 2009). For all localities investigated
220 in this study, $R_{cpx/opx}$ fall within these established ranges, indicating equilibrium **(Fig. 4).**
221
222 ***Xenolith NAM water contents***
223 Although Siberian xenoliths report very high measured olivine water contents (>300 ppm
224 at 7 GPa, 1250 °C), RC values for these olivines are much lower than measured values
225 **(Fig. 2, SI Table 3)**. Such a large negative difference in RC versus measured olivine H_2O
226 content could indicate re-hydration of olivine during eruption or during emplacement, or
227 anomalously high olivine water content due to metasomatism shortly before eruption.
228 However, $R_{cpx/opx}$ for Siberian xenoliths (0.91 ± 0.32) is close to experimental D values
229 (1.3 ± 0.3) **(Fig. 4),** indicating that the pyroxenes retained an equilibrium state. Kaapvaal
230 xenoliths have an average RC olivine H_2O content of 25 ppm and show a smaller

231 dispersion of ΔH_2O **(Fig. 2)** compared to those from Siberia; Kaapvaal xenoliths also
232 have $R_{cpx/opx}$ within the range of experimental D values (1.72 ± 0.4) **(Fig. 4)**. The
233 Wyoming Craton has the highest RC olivine H_2O out of all cratons (39 ppm), $R_{cpx/opx}$ is
234 within the experimental range (1.6 ± 0.35), and generally shows a positive ΔH_2O. Finally,
235 the craton-like Proterozoic Colorado Plateau is characterized by unusually high RC
236 olivine water contents attributed to Cenozoic flat slab subduction and metasomatism (Li
237 et al., 2008) **(Fig. 2)**.

238 Measured orthopyroxene water contents are shown in **Fig. 3b** for the same
239 xenoliths for which RC olivine water contents are reported. As clinopyroxene water
240 contents show a similar distribution to values for orthopyroxene in **Fig. 3a**, we only show
241 orthopyroxene for simplicity. In general, orthopyroxene water content does not show a
242 marked increase with increasing depth.

243 In contrast to cratons, non-cratonic mantle xenoliths show RC olivine water
244 contents that are higher than measured values **(Fig. 2)**. Notably, neither olivine nor
245 orthopyroxene in xenoliths from lithospheric mantle above subduction zones (Simcoe,
246 Mexico, and Sierra Nevada) are particularly more hydrous than those in xenoliths from
247 the Basin and Range and cratons.

248

249 **DISCUSSION**

250 ***A consistent level of olivine water undersaturation in the lithospheric mantle?***

251 Although our method of pyroxene-anchored recalculation of olivine water
252 contents usually yields a higher value than the observed water content **(Fig. 2b)**, it is
253 possible that even these values may be a minimum bound on the last water content

representative of the lithospheric mantle. Recent work comparing spectroscopic versus bulk methods of analyzing water in NAMs shows higher values using bulk methods, suggesting there may be "missing" water stored in minerals, perhaps as molecular H_2 (Moine et al., 2020). In addition, water freed during metamorphic reactions in the deep lithosphere could also form hydro-garnet, which is undetectable during routine petrographic study (Lamadrid et al., 2014). Despite these uncertainties, the RC values we report are internally consistent with coexisting pyroxenes, and thus reflect the last water content of the lithospheric mantle prior to eruption.

When the RC olivine water contents are plotted as a function of depth **(Fig. 3)**, we find a relatively constant value around 30 ppm **(Fig. 2)**. This holds across cratonic versus off-cratonic boundaries – the average RC olivine is 28 ± 18 ppm for cratonic xenoliths (Siberia, Kaapvaal, Wyoming, North China, Colorado Plateau) and 26 ± 12 ppm for off-cratonic xenoliths (Simcoe, Mexico, Sierra Nevada, Basin and Range). Such a consistent RC olivine water content may reflect a universal equilibrated state of water undersaturation in the background lithospheric mantle. Interestingly, the observation that global olivine has recalculated water contents around 30–40 ppm could also reconcile why a large number of mantle xenoliths with "dry" A-type fabric often contain large populations of "wet" E-type intragranular microstructures (Bernard et al., 2019; Chin et al., 2021), since this water content is at the boundary between the two olivine fabric types (Karato et al., 2008).

Implications for cratonization processes

P-T paths and water "sweating"

Various aspects of mineral-based thermobarometry should be considered when interpreting thermal histories of xenoliths with respect to the hydration state of the lithosphere, because the solubility of volatiles is strongly pressure and temperature dependent. Most *P*–*T* conditions of equilibration of peridotites are constrained simultaneously using Al-in-orthopyroxene barometry coupled with Mg, Fe, or Ca-based cation exchange thermometry between garnet and orthopyroxene or clinopyroxene. However, because Al^{3+} diffusivity is much slower than that of divalent cations at temperatures of the cool lithospheric mantle (Cherniak and Dimanov, 2010), transient thermal events may shift previously equilibrated xenoliths off the geotherm, leading to spurious calculated *P*–*T* arrays (Lee, 1998). Large temperature shifts will thus significantly affect the potential water capacity of a NAM, allowing it to release and redistribute previously incorporated water into the surrounding matrix or consume more in post-formation hydration events **(Fig. 1)**.

This issue may be particularly important for Al solubility in mantle minerals, especially for metamorphic reactions involving pyroxenes and garnet. Owing to the positive dP/dT slope of the spinel-garnet transition, garnet inevitably forms during isobaric cooling **(Fig. 5a)** at high pressure subsolidus conditions of the cratonic lithospheric mantle. H^+ participates in a coupled substitution with Al^{3+} in orthopyroxene (Keppler and Bolfan-Casanova, 2006), and so the behavior of Al^{3+} in the lithospheric mantle should also impact its water content and distribution. Studies of cratonic peridotites show that garnet and clinopyroxene are often spatially associated with orthopyroxene (Cox et al., 1987; Saltzer et al., 2001; Tomlinson et al. 2017), with the former occurring as lamellae within the latter. This led to the idea that garnet and

clinopyroxene may have exsolved as a result of cooling from originally homogenous high-*T*, low-*P*, and high-Al orthopyroxene (Cox et al., 1987). Exsolution-induced water release could therefore be significant for Al-enstatite, which can theoretically hold similar concentrations of H^+ as olivine at high temperatures **(Fig. 1)**, and which participates in the metamorphic garnet-forming reaction during cooling and/or increasing pressure **(Fig. 5a)**. Because garnet has much lower D_{H2O} compared to pyroxene (Hauri et al., 2006; Tenner et al., 2009), garnet formation from orthopyroxene should thus release water into the host peridotite, which may then be taken up by clinopyroxene, which has a higher D_{H2O}, or react to form amphibole. We propose that the down-temperature increase in $R_{cpx/opx}$ **(Fig. 4)** may partially reflect closed-system re-partitioning of water into clinopyroxene as orthopyroxene exsolves garnet.

The Sierra Nevada mantle as an analog for cratonic lithosphere formation

One example of potential cooling-induced water exsolution due to garnet formation from orthopyroxene is recorded by peridotite xenoliths from the Sierra Nevada, California (Chin et al., 2012). Although the Sierra Nevada formed as a Mesozoic arc, several aspects of its lithospheric evolution are reminiscent of the cratonic lithosphere (Lee et al., 2011; Gibson, 2017). These include equilibration of Sierran peridotite xenoliths along an anomalously cold geotherm similar to cratonic conditions, and recording final pressures up to ~4 GPa (Ducea and Saleeby, 1996), similar to cratonic xenoliths. The inferred *P-T* path **(Fig. 5a)** of the Sierran peridotites is interpreted to represent significant tectonic thickening in a compressional subduction zone (Chin et al., 2012). Following melt depletion and subsequently during deformation and thickening,

the Sierran mantle was melt-infiltrated and hydrated (Lee, 2005; Chin et al., 2014). The final equilibration at low temperatures (<800 °C) and high pressures (3-4 GPa), together with rapid cooling to "lock" in chemical and textural evidence, preserved garnet exsolution lamellae in orthopyroxene grains (Chin et al., 2014). Furthermore, rapid thickening and cooling may have promoted minor exsolution of water from olivine to form amphibole replacing clinopyroxene (Chin et al., 2016). In fact, Chin et al. (2016) found that the observed discrepancy between measured olivine water content versus clinopyroxene-recalculated (i.e., RC) olivine water content could actually account for the "missing water" needed to form the observed amphibole, further bolstering an exsolution hypothesis. In **Fig. 4a,** the Sierran xenoliths plot at the lowest temperatures and have the highest $R_{cpx/opx}$, consistent with subsolidus re-equilibration and re-distribution of water between pyroxenes.

The need for an early re-hydration process during cratonization

Exsolution-induced garnet formation and associated water release from orthopyroxene in melt-depleted peridotites, alone, is unlikely to account for the puzzling occurrence of garnet harzburgite in the cratonic lithosphere. Metasomatism is usually required to explain the observed proportions of garnet and clinopyroxene compared to the volumes expected for melt-depleted peridotite, as well as the mineralogical heterogeneity observed in xenoliths sampled at different depths. Yet, a balance must be struck between "ad hoc" metasomatism, which re-introduces major elements, volatiles, heat-producing incompatible elements and thus will reheat and redensify the mantle, and the apparent long-term preservation of stable, thick, cold cratonic mantle lithosphere (Rudnick et al.,

1998). We propose that metasomatism occurring early in the cratonization process – for example, while initially melt-depleted residues undergo thickening, deformation, and stabilization, as discussed above in the Sierra Nevada case – could re-introduce volatiles into a rock matrix during retrograde metamorphism, after which exsolution-induced garnet formation and water release due to decreased temperatures and increased pressures results in water re-distribution.

Our argument stems from the geophysical imaging showing that many cratons contain complex internal structure, such as dipping layers reminiscent of subducted slabs (Mercier et al., 2008) or suture zones formed via continent–continent collision (**Fig. 5b)**. This indicates that these cratons likely formed due to mobile lid tectonics, which have operated at an increasingly global scale since at least the Mesoarchean (Palin and Santosh, 2020). Owing to their cold, highly viscous states, it is unlikely that significant deformation occurred in most cratons after their initial formation, although, the disturbed Wyoming and North China Cratons are notable exceptions (Liu et al., 2018). Thus, the presence of intra-cratonic layering and/or past plate boundaries suggests that cratonic nuclei were initially mobile and deformed during coalescence in the Archean – Proterozoic to generate such structures (Capitanio et al., 2020).

One way to enhance deformation in mantle rock is to add water, which has a weakening effect and lowers viscosity (Hirth and Kohlstedt, 1996) and enhances creep rate (Karato et al., 1986). Rehydration may therefore allow previously melt-depleted cratonic nuclei to deform while forming thick roots. Too much hydration, however, would impede preservation, owing to the low viscosity conferred by hydration. By contrast, mantle lithosphere that is too dry will have difficulty in localizing shear zones

and promoting ongoing deformation to form cratonic nuclei. One potential scenario is heterogeneous distribution of water in the mantle lithosphere, perhaps localized in fossil shear zones (Speciale et al., 2020), which we discuss further below.

Syn-cratonization scenarios that could rehydrate proto-cratonic roots as they deform and thicken into keels include serpentinization and refertilization. If cratons form by imbrication of oceanic slabs **(Fig. 4b)**, (re)hydration could occur by serpentinization. In fact, serpentinization has been called upon to explain Si-enrichment observed beneath the Kaapvaal Craton (Canil and Lee, 2009). Refertilization during thickening, via melt infiltration and hydration (cf., Chin et al., 2012), may be another way to re-introduce volatiles. We propose that syn-cratonization rehydration/refertilization, akin to the process described earlier in this paper for the Sierra Nevada, could have also been favorable for development of deep lithospheric shear zones (e.g. Dijkstra et al., 2002). In experiments on an H_2O-saturated, olivine-rich shear zone (1.2 GPa, 900 °C), Precigout et al. (2019) found high H_2O content in olivine in areas where shear strain was localized. The observed H_2O amounts exceeded the predicted amount for grain boundary saturation; instead, cavitation rate may increase with strain rate, resulting in progressive H_2O transfer from low to high strain zones.

Initially small grain size and high water contents could facilitate early strain localization and craton mobility, perhaps aiding the several 100's of Ma timescales needed for craton coalescence. Grain size in shear zones and mylonites tends to be reduced because dynamic recrystallization promotes weakening; but, grain growth (static recrystallization) counteracts this process (Montesi and Hirth, 2003). In fact, olivine grain growth takes far longer if the grains are "damp" as opposed to being water-

saturated (Speciale et al., 2020). Damp, rather than water-saturated or completely dry, olivine and pyroxene could be prevalent shortly following syn-cratonization rehydration, boosting the originally depleted mantle lithosphere's water content. Following the final cooling and stabilization of the craton, this re-introduced water would exsolve from orthopyroxene during garnet formation. Olivine would also exsolve water due to the reduced solubility at decreased temperature, increasing mantle viscosity and ending this initial window of craton deformation. The slowing of grain growth with decreased water content and this inherited heterogeneity of water distribution in the lithosphere could also explain why, despite average coarse (~1 cm) grain sizes, cratonic peridotites of various grain sizes and textures are still sampled in geologically recent kimberlites.

In summary, we propose that "sweating" of lithospheric water during cratonization could explain the roughly constant 30 ppm last water content observed in mantle olivines. In addition, the increase of Rcpx/opx with decreasing temperature, particularly for cratonic regions **(Fig. 4)**, is consistent with the subsolidus re-distribution of water into clinopyroxene compared to orthopyroxene. This may occur as orthopyroxene exsolves garnet, releasing water which would favor to enter clinopyroxene due to its higher D relative to garnet, olivine, and orthopyroxene.

Speculations on the origin of the mid-lithospheric discontinuity

Finally, our data compilation and forward modeling may shed new light on the origin of the so-called "mid-lithospheric discontinuity" (MLD), which has been identified through seismic shear wave receiver function studies performed on all major continents on Earth (e.g. Selway et al., 2015). Vertical seismic velocity profiles consistently observe a

significant decrease in P- and S-wave velocities at depths of ~60–160 km, although this is most pronounced at ~80–100 km. In regions that are tectonically active, this is often interpreted as representing the lithosphere–asthenosphere boundary (LAB: Ford et al., 2010); however, in stable continental and cratonic regions, the LAB may be as deep as 300 km (Artemieva and Mooney, 2001; Kind et al., 2012), and the continuity of this low-velocity band through the lithosphere is more difficult to explain. Some previous studies have invoked the presence of concentrated partial melt at MLD depths (Thybo and Perchuc, 1997), an up-temperature transition in olivine deformation behavior from elastic to anelastic that promotes grain boundary sliding and bulk-rock weakening (Karato, 2012), or compositional gradients that produce different mineral assemblages above and below the MLD, such as bulk-peridotite Mg# (Yuan and Romanowicz, 2010).

An intriguing extension of the latter hypothesis is that the MLD may be caused by a hydrated layer within the lithosphere, either caused by small concentrations of hydrous minerals (phlogopite, amphibole) or wetter olivine compared to ambient lithospheric mantle (Liu et al., 2018). Geochemical calculations performed by Selway et al. (2015) showed that infiltration of water into pyrolite at various depths across the MLD produced sufficient volumes of amphibole and phlogopite to reduce the bulk-rock seismic velocity and replicate the MLD. In addition, Eeken et al. (2018) calculated that even 0.25 wt.% H_2O added to peridotite already produces ~13 % of a hydrous mineral assemblage in the host peridotite, which is on the high end for generally "depleted" cratonic mantle.

However, to date, most or all such studies invoke post-cratonization metasomatism to explain a hydration origin for the MLD. Instead, we argue that our mechanism of early, syn-cratonization rehydration/refertilization followed by cooling-

induced water exsolution from NAMs may release, at minimum, 100's of ppm of water *per mineral*. This may be further facilitated along favorable P-T paths such as (3) in **Fig. 5a**, wherein mantle is thickened isothermally (i.e., during rapid tectonic or magmatic thickening) and then cooled isobarically into the garnet stability field. In fact, the sharpest decreases in water solubility in olivine and orthopyroxene along the three geotherms discussed above are predicted at pressures of 2.5–3.5 GPa just below the solidus **(Fig. S1)**, which is equivalent to 90–120 km depth below the Earth's surface. We propose that "sweating" of water in the deep lithosphere due to changing P-T conditions and hence solubility during cratonization may have been a ubiquitous phenomenon in the early Earth, and circumvents the issue of different cratons having different geological histories. Our hypothesis provides a self-consistent cratonization model that does not necessistate *ad hoc* metasomatism post-dating craton formation to explain intra-cratonic layering.

CONCLUSIONS

New thermodynamically constrained models of NAM water storage capacities for pyrolite and garnet harzburgite at 0–5 GPa and 600–1600 °C show that cratonic mantle can potentially hold up to ~2000 ppm H_2O along typical geotherms. When comparing these predicted capacities with published data, we show that: 1) recalculated olivine water contents to be in equilibrium with clinopyroxene are consistent regardless of tectonic setting, implying that global lithospheric mantle reflects an equilibrium level of undersaturation (~10-times lower than its potential storage capacity), 2) pyroxene-measured water contents reflect undersaturation (about ~2 times relative to maximum

storage capacity), and 3) the ratio of water that can be incorporated in clinopyroxene/orthopyroxene increases with decreasing temperature. These models provide a quantitative framework onto which future investigations of NAM research can build. In particular, knowledge of xenolith *P*–*T* history may be used to quantify the potential magnitude of fluid release, and our calculated values may allow for predictive modeling of subsolidus (re-)partitioning of water in different tectonic settings throughout geological time. Cooling may thus dynamically drive devolatilization and self-catalyze mineralogical transformation, eliminating the need for invoking *ad hoc* hydration events driven by externally derived aqueous fluids, which are often suggested to explain the trace element and volatile characteristics of many cratonic xenoliths.

DATA AVAILABILITY

All data used in this work are provided in Table S3 or can be found in articles referenced in the main text.

FIGURES

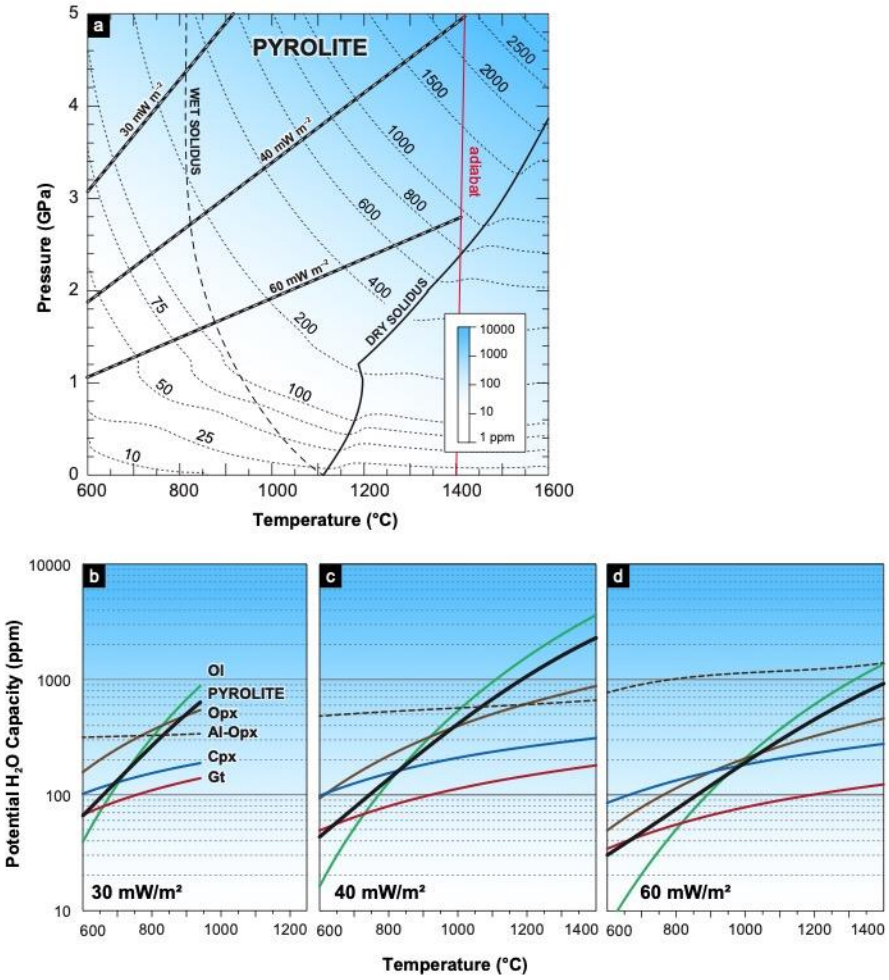

480

481 **Figure 1. Modeled H_2O storage.** A) Potential H_2O capacity for pyrolite at *P–T*

482 conditions of the cratonic mantle. B-D) H_2O capacity in NAMs and bulk pyrolite along

483 typical mantle geotherms.

484

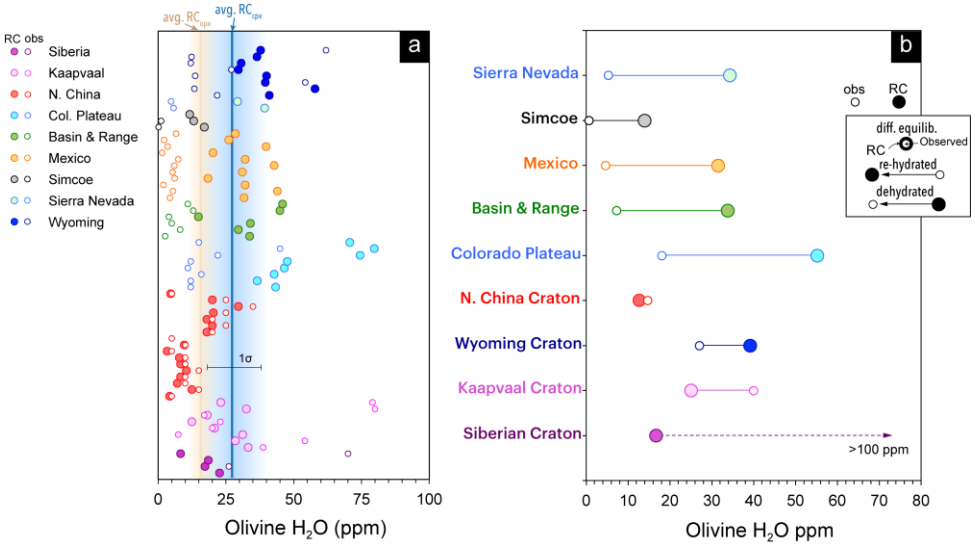

Figure 2. Literature xenolith data. A) Individual xenoliths with previously published coexisting olivine, clinopyroxene, and orthopyroxene water contents (see SI for references). All data plotted are olivine water contents. Open symbols = observed (i.e., measured) olivine water content. Filled symbols = olivine water contents recalculated to clinopyroxene water content (RC). Vertical bold lines represent average recalculated olivine water contents (all xenolith data). B) Comparison between RC and observed olivine water contents. Symbols represent averages for each locality. Inset shows that positive or negative differences in RC vs. observed values could indicate dehydration and rehydration, respectively.

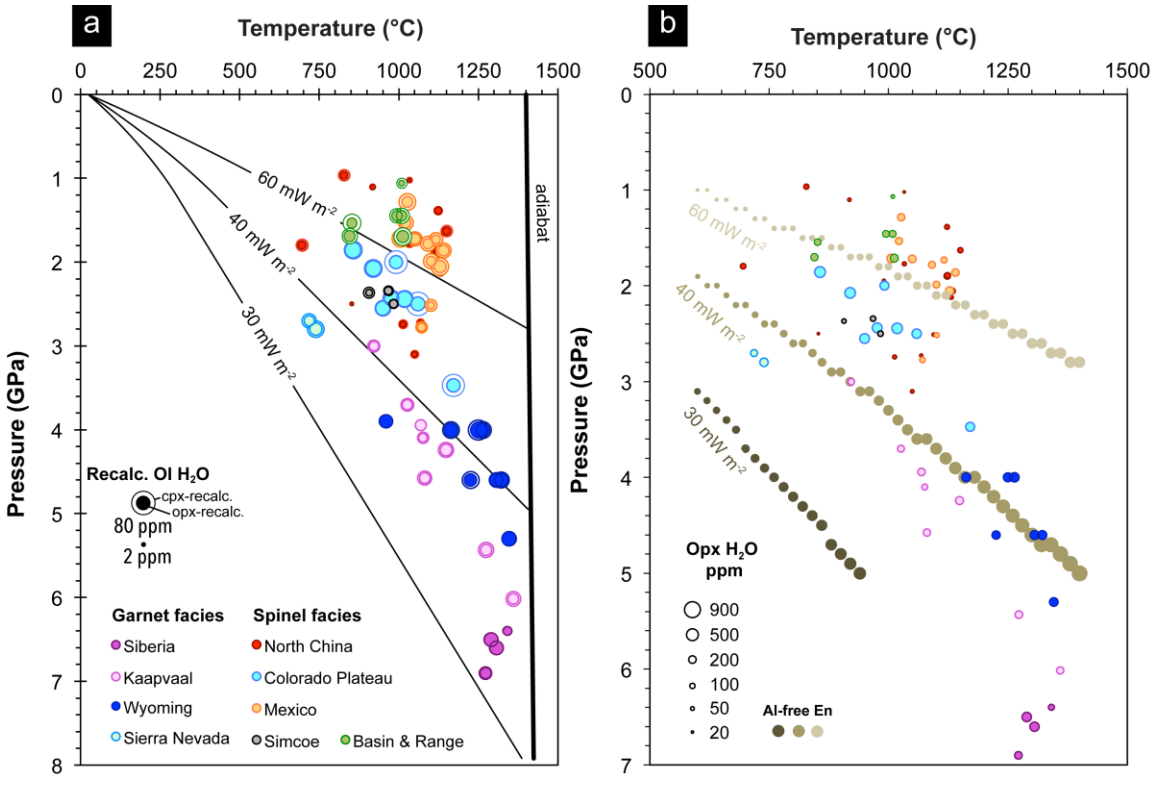

Figure 3. A) RC olivine H_2O in *P–T* space. B) Measured orthopyroxene H_2O in *P–T* space. Brown circles are modeled orthopyroxene H_2O storage capacities along different model geotherms (from **Fig. 1**).

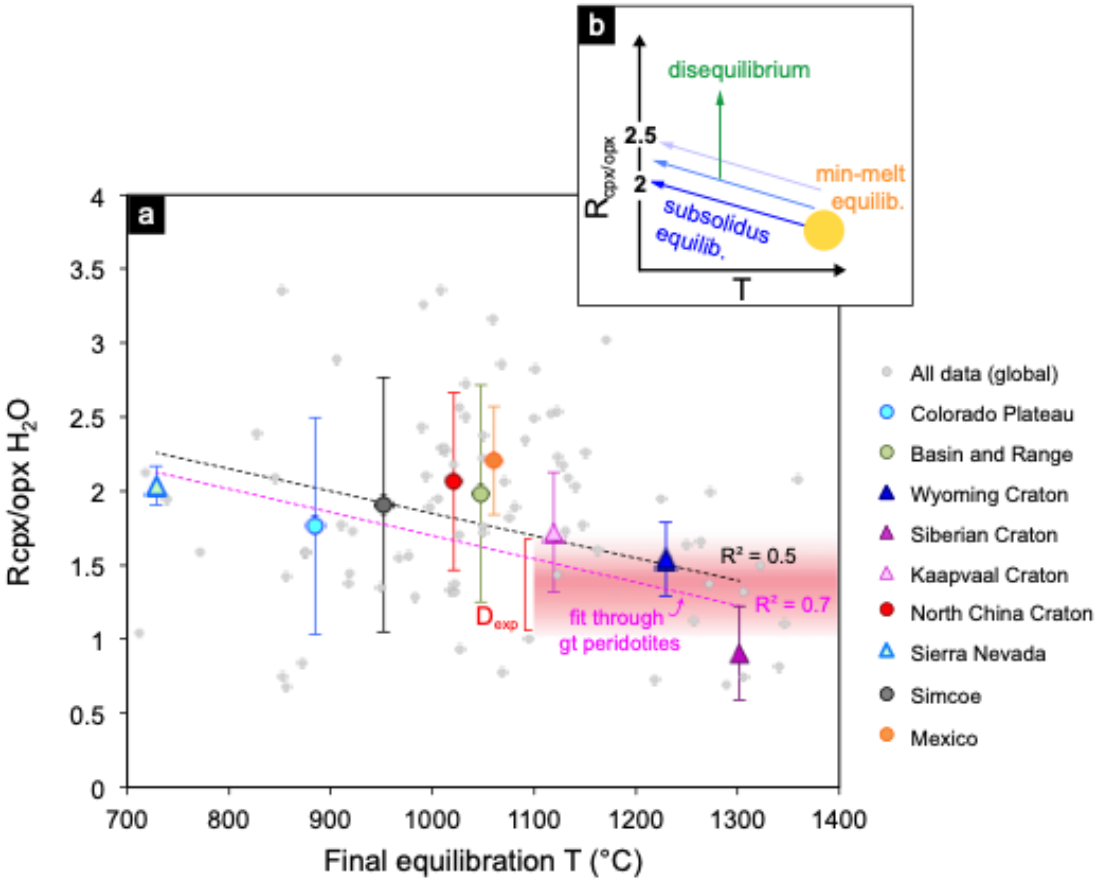

Figure 4. (A) Ratio of measured H_2O in clinopyroxene/orthopyroxene vs. final equilibration T in mantle xenoliths. Error bars 1σ. Dashed lines show regressions through global data (black) and garnet peridotites only (magenta). (B) Potential mechanisms responsible for shifts in R.

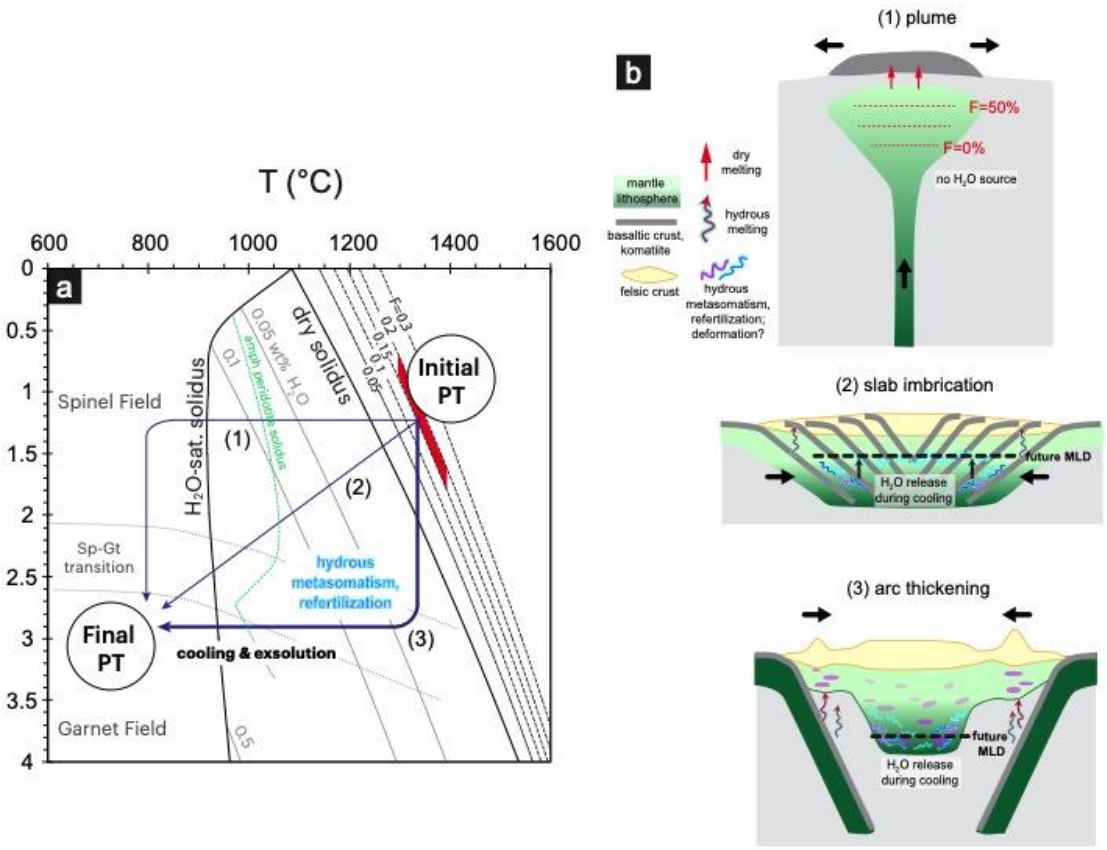

506

507 **Figure 5.** A) *P–T* diagram after Chin et al. (2012) and Lee and Chin (2014) showing
508 paths of mantle lithosphere starting from shallow, high-T melt depletion and subsequent
509 cooling and thickening. B) Cratonization models based on Lee et al. (2011). Cooling-
510 induced hydration to form lithospheric discontinuities is shown.

511

512 **REFERENCES**

513 1. Artemieva, I.M. and Mooney, W.D., 2001. Thermal thickness and evolution of
514 Precambrian lithosphere: A global study. Journal of Geophysical Research: Solid
515 Earth, 106(B8), pp.16387-16414.

2. Aubaud, C., Hauri, E. H., and Hirschmann, M. M., 2004, Hydrogen partition coefficients between nominally anhydrous minerals and basaltic melts: Geophysical Research Letters, v. 31, no. 20.
3. Bell, D. R., and Rossman, G. R., 1992, Water in Earth's mantle: the role of nominally anhydrous minerals: Science, v. 255, no. 5050, p. 1391-1397.
4. Bernard, R. E., Behr, W. M., Becker, T. W., and Young, D. J., 2019, Relationships between olivine CPO and deformation parameters in naturally deformed rocks and implications for mantle seismic anisotropy: Geochemistry, Geophysics, Geosystems.
5. Bodnar, R.J., Azbej, T., Becker, S.P., Cannatelli, C., Fall, A. and Severs, M.J., 2013. Whole Earth geohydrologic cycle, from the clouds to the core: The distribution of water in the dynamic Earth system. The Geological Society of America Special Paper, 500, pp.431-61.
6. Brodholt, J.P., Refson, K., 2000. An ab initio study of hydrogen in forsterite and a possible mechanism for hydrolytic weakening. Journal of Geophysical Research: Solid Earth 105, 18977-18982.
7. Canil, D., and Lee, C.-T. A., 2009, Were deep cratonic mantle roots hydrated in Archean oceans?: Geology, v. 37, no. 7, p. 667-670.
8. Capitanio, F.A., Nebel, O. and Cawood, P.A., 2020. Thermochemical lithosphere differentiation and the origin of cratonic mantle. Nature, 588(7836), pp.89-94.
9. Cherniak, D.J. and Dimanov, A., 2010. Diffusion in pyroxene, mica and amphibole. Reviews in Mineralogy and Geochemistry, 72(1), pp.641-690.

10. Chin, E.J., Chilson-Parks, B., Boneh, Y., Hirth, G., Saal, A., Hearn, B.C., Hauri, E., 2021. The peridotite deformation cycle in cratons and the deep impact of subduction. Tectonophysics, 229029 (in press).
11. Chin, E. J., Lee, C.-T. A., Luffi, P., and Tice, M., 2012, Deep Lithospheric Thickening and Refertilization beneath Continental Arcs: Case Study of the P, T and Compositional Evolution of Peridotite Xenoliths from the Sierra Nevada, California: Journal of Petrology, v. 53, no. 3, p. 477-511.
12. Chin, E. J., Lee, C. T. A., and Blichert-Toft, J., 2015, Growth of upper plate lithosphere controls tempo of arc magmatism: Constraints from Al-diffusion kinetics and coupled Lu-Hf and Sm-Nd chronology: Geochemical Perspectives Letters, v. 1, no. 0, p. 20-32.
13. Chin, E. J., Soustelle, V., Hirth, G., Saal, A., Kruckenberg, S. C., and Eiler, J., 2016, Microstructural and geochemical constraints on the evolution of deep arc lithosphere: Geochemistry, Geophysics, Geosystems, v. 17, no. 7, p. 2497-2521.
14. Condie, K.C., 2021. Two Major Transitions in Earth History: Evidence of Two Lithospheric Strength Thresholds. The Journal of Geology 129, 455-473.
15. Cox, K. G., Smith, M. R., and Beswetherick, S., 1987, Textural studies of garnet lherzolites: evidence of exsolution origin from high-temperature harzburgites, *in* Nixon, P. H., ed., Mantle Xenoliths, John Wiley and Sons Ltd.
16. de Capitani, C., and Petrakakis, K., 2010, The computation of equilibrium assemblage diagrams with Theriak/Domino software: American Mineralogist, v. 95, no. 7, p. 1006-1016.

17. Demouchy, S., and Bolfan-Casanova, N., 2016, Distribution and transport of hydrogen in the lithospheric mantle: A review: Lithos, v. 240, p. 402-425.
18. Demouchy, S., Shcheka, S., Denis, C. M., and Thoraval, C., 2017, Subsolidus hydrogen partitioning between nominally anhydrous minerals in garnet-bearing peridotite: American Mineralogist, v. 102, no. 9, p. 1822-1831.
19. Dijkstra, A.H., Drury, M.R., Vissers, R.L. and Newman, J., 2002. On the role of melt-rock reaction in mantle shear zone formation in the Othris Peridotite Massif (Greece). Journal of Structural Geology, 24(9), pp.1431-1450.
20. Ducea, M.N., Saleeby, J.B., 1996. Buoyancy sources for a large, unrooted mountain range, the Sierra Nevada, California: Evidence from xenolith thermobarometry. J. Geophys. Res. 101, 8229-8244.
21. Eeken, T., Goes, S., Pedersen, H. A., Arndt, N. T., and Bouilhol, P., 2018, Seismic evidence for depth-dependent metasomatism in cratons: Earth and Planetary Science Letters, v. 491, p. 148-159.
22. Ford, H.A., Fischer, K.M., Abt, D.L., Rychert, C.A. and Elkins-Tanton, L.T., 2010. The lithosphere–asthenosphere boundary and cratonic lithospheric layering beneath Australia from Sp wave imaging. Earth and Planetary Science Letters, 300(3-4), pp.299-310.
23. Ganne, J., Feng, X., 2017. Primary magmas and mantle temperatures through time. Geochemistry, Geophysics, Geosystems 18, 872-888.
24. Gibson, S. A., 2017, On the nature and origin of garnet in highly-refractory Archean lithospheric mantle: constraints from garnet exsolved in Kaapvaal craton orthopyroxenes: Mineralogical Magazine, v. 81, no. 4, p. 781-809.

25. Hauri, E. H., Gaetani, G. A., and Green, T. H., 2006, Partitioning of water during melting of the Earth's upper mantle at H 2 O-undersaturated conditions: Earth and Planetary Science Letters, v. 248, no. 3, p. 715-734.
26. Herzberg, C., Condie, K. and Korenaga, J., 2010. Thermal history of the Earth and its petrological expression. Earth and Planetary Science Letters, 292(1-2), pp.79-88.
27. Hirth, G. and Kohlstedt, D.L., 1996. Water in the oceanic upper mantle: implications for rheology, melt extraction and the evolution of the lithosphere. Earth and Planetary Science Letters, 144(1-2), pp.93-108.
28. Hirschmann, M. M., 2006, Water, melting, and the deep Earth H_2O Cycle: Annual Review of Earth and Planetary Sciences, v. 34, no. 1, p. 629-653.
29. Hoal, K.E.O., Hoal, B.G., Erlank, A.J. and Shimizu, N., 1994. Metasomatism of the mantle lithosphere recorded by rare earth elements in garnets. Earth and Planetary Science Letters, 126(4), pp.303-313.
30. Holland, T. J. B., and Powell, R., 2011, An improved and extended internally consistent thermodynamic dataset for phases of petrological interest, involving a new equation of state for solids: Journal of Metamorphic Geology, v. 29, no. 3, p. 333-383.
31. Jennings, E. S., and Holland, T. J., 2015, A simple thermodynamic model for melting of peridotite in the system NCFMASOCr: Journal of Petrology, v. 56, no. 5, p. 869-892.

32. Jordan, T.H., 1981. Continents as a chemical boundary layer. Philosophical Transactions of the Royal Society of London. Series A, Mathematical and Physical Sciences, 301(1461), pp.359-373.
33. Karato, S.I., 2012. On the origin of the asthenosphere. Earth and Planetary Science Letters, 321, pp.95-103.
34. Karato, S.-i., Jung, H., Katayama, I., and Skemer, P., 2008, Geodynamic significance of seismic anisotropy of the upper mantle: new insights from laboratory studies: Annu. Rev. Earth Planet. Sci., v. 36, p. 59-95.
35. Keppler, H., and Bolfan-Casanova, N., 2006, Thermodynamics of water solubility and partitioning: Reviews in Mineralogy and Geochemistry, v. 62, no. 1, p. 193-230.
36. Kind, R., Yuan, X., Kumar, P., 2012. Seismic receiver functions and the lithosphere–asthenosphere boundary. Tectonophysics 536, 25-43.
37. Kopylova, M. G., and Russell, J. K., 2000, Chemical stratification of cratonic lithosphere: constraints from the Northern Slave craton, Canada: Earth and Planetary Science Letters, v. 181, no. 1,Äì2, p. 71-87.
38. Lamadrid, H., Lamb, W., Santosh, M., Bodnar, R., 2014. Raman spectroscopic characterization of H2O in CO2-rich fluid inclusions in granulite facies metamorphic rocks. Gondwana Research 26, 301-310.
39. Lee, C., 1998. Are inflected geotherms real?, International Kimberlite Conference: Extended Abstracts, pp. 489-491.

625 40. Lee, C.T.A., 2005. Trace element evidence for hydrous metasomatism at the base
626 of the North American lithosphere and possible association with Laramide low-
627 angle subduction. The Journal of Geology, 113(6), pp.673-685.
628 41. Lee, C.-T.A., Luffi, P., Höink, T., Li, Z.-X.A., Lenardic, A., 2008. The role of
629 serpentine in preferential craton formation in the late Archean by lithosphere
630 underthrusting. Earth and Planetary Science Letters 269, 96-104.
631 42. Lee, C.-T. A., and Chin, E. J., 2014, Calculating melting temperatures and
632 pressures of peridotite protoliths: Implications for the origin of cratonic mantle:
633 Earth and Planetary Science Letters, v. 403, p. 273-286.
634 43. Lee, C.-T. A., Luffi, P., and Chin, E. J., 2011, Building and Destroying
635 Continental Mantle: Annual Review of Earth and Planetary Sciences, v. 39, no. 1.
636 44. Li, Z.-X. A., Lee, C.-T. A., Peslier, A. H., Lenardic, A., and Mackwell, S. J.,
637 2008, Water contents in mantle xenoliths from the Colorado Plateau and vicinity:
638 Implications for the mantle rheology and hydration-induced thinning of
639 continental lithosphere: Journal of Geophysical Research: Solid Earth, v. 113, no.
640 B9, p. n/a-n/a.
641 45. Liu, L., Morgan, J.P., Xu, Y., Menzies, M., 2018. Craton destruction 1: Cratonic
642 keel delamination along a weak midlithospheric discontinuity layer. Journal of
643 Geophysical Research: Solid Earth 123, 10,040-010,068.
644 46. Mackwell, S.J. and Kohlstedt, D.L., 1990. Diffusion of hydrogen in olivine:
645 implications for water in the mantle. Journal of Geophysical Research: Solid
646 Earth, 95(B4), pp.5079-5088.

47. Mercier, J. P., Bostock, M., Audet, P., Gaherty, J., Garnero, E., and Revenaugh, J., 2008, The teleseismic signature of fossil subduction: Northwestern Canada: Journal of Geophysical Research: Solid Earth, v. 113, no. B4.
48. Mierdel, K., Keppler, H., Smyth, J. R., and Langenhorst, F., 2007, Water solubility in aluminous orthopyroxene and the origin of Earth's asthenosphere: Science, v. 315, no. 5810, p. 364-368.
49. Moine, B., Bolfan-Casanova, N., Radu, I., Ionov, D., Costin, G., Korsakov, A., Golovin, A., Oleinikov, O., Deloule, E., Cottin, J., 2020. Molecular hydrogen in minerals as a clue to interpret∂ D variations in the mantle. Nature communications 11, 1-10.
50. Montési, L.G. and Hirth, G., 2003. Grain size evolution and the rheology of ductile shear zones: from laboratory experiments to postseismic creep. Earth and Planetary Science Letters, 211(1-2), pp.97-110.
51. Nicoli, G., Ferrero, S., 2021. Nanorocks, volatiles and plate tectonics. Geoscience Frontiers 12, 101188.
52. O'Leary, J. A., Gaetani, G. A., and Hauri, E. H., 2010, The effect of tetrahedral Al3+ on the partitioning of water between clinopyroxene and silicate melt: Earth and Planetary Science Letters, v. 297, no. 1–2, p. 111-120.
53. Palin, R. M., and Santosh, M., 2020, Plate tectonics: What, where, why, and when?: Gondwana Research.
54. Palin, R.M., Santosh, M., Cao, W., Li, S.S., Hernández-Uribe, D. and Parsons, A., 2020. Secular change and the onset of plate tectonics on Earth. Earth-Science Reviews, 207, p.103172.

55. Palin, R.M. and White, R.W., 2016. Emergence of blueschists on Earth linked to secular changes in oceanic crust composition. Nature Geoscience, 9(1), pp.60-64.
56. Pearson, D.G., Scott, J.M., Liu, J., Schaeffer, A., Wang, L.H., van Hunen, J., Szilas, K., Chacko, T. and Kelemen, P.B., 2021. Deep continental roots and cratons. Nature, 596(7871), pp.199-210.
57. Peslier, A.H., 2010. A review of water contents of nominally anhydrous natural minerals in the mantles of Earth, Mars and the Moon. Journal of Volcanology and Geothermal Research 197, 239-258.
58. Peslier, A.H., Schönbächler, M., Busemann, H. and Karato, S.I., 2017. Water in the Earth's interior: Distribution and origin. Space Science Reviews, 212(1), pp.743-810.
59. Pearson, D., Canil, D., Shirey, S., 2003. Mantle samples included in volcanic rocks: xenoliths and diamonds. Treatise on Geochemistry 2, 171-275.
60. Piccolo, A., Kaus, B.J., White, R.W., Palin, R.M. and Reuber, G.S., 2020. Plume—Lid interactions during the Archean and implications for the generation of early continental terranes. Gondwana Research, 88, pp.150-168.
61. Pollack, H.N., Chapman, D.S., 1977. On the regional variation of heat flow, geotherms, and lithospheric thickness. Tectonophysics 38, 279-296.
62. Précigout, J., Stünitz, H. and Villeneuve, J., 2019. Excess water storage induced by viscous strain localization during high-pressure shear experiment. Scientific reports, 9(1), pp.1-9.
63. Ringwood, A. E., 1975, Composition and Petrology of the Earth's Mantle: MacGraw-Hill, v. 618.

64. Rudnick, R.L., McDonough, W.F. and O'Connell, R.J., 1998. Thermal structure, thickness and composition of continental lithosphere. *Chemical Geology*, *145*(3-4), pp.395-411.

65. Saltzer, R. L., Chatterjee, N., and Grove, T. L., 2001, The Spatial Distribution of Garnets and Pyroxenes in Mantle Peridotites: Pressure-Temperature History of Peridotites from the Kaapvaal Craton: Journal of Petrology, v. 42, no. 12, p. 2215-2229.

66. Selway, K., Ford, H. and Kelemen, P., 2015. The seismic mid-lithosphere discontinuity. Earth and Planetary Science Letters, 414, pp.45-57.

67. Speciale, P.A., Behr, W.M., Hirth, G. and Tokle, L., 2020. Rates of olivine grain growth during dynamic recrystallization and postdeformation annealing. Journal of Geophysical Research: Solid Earth, 125(11), p.e2020JB020415.

68. Tenner, T. J., Hirschmann, M. M., Withers, A. C., and Hervig, R. L., 2009, Hydrogen partitioning between nominally anhydrous upper mantle minerals and melt between 3 and 5 GPa and applications to hydrous peridotite partial melting: Chemical Geology, v. 262, no. 1, p. 42-56.

69. Tomlinson, E.L., Kamber, B.S., Hoare, B.C., Stead, C.V. and Ildefonse, B., 2018. An exsolution origin for Archean mantle garnet. *Geology*, *46*(2), pp.123-126.

70. Thybo, H. and Perchuć, E., 1997. The seismic 8 discontinuity and partial melting in continental mantle. Science, 275(5306), pp.1626-1629.

71. Tian, Z.Z., Liu, J., Xia, Q.K., Ingrin, J., Hao, Y.T. and Christophe, D., 2017. Water concentration profiles in natural mantle orthopyroxenes: A geochronometer for long annealing of xenoliths within magma. Geology, 45(1), pp.87-90.

72. Ulmer, P., 2001, Partial melting in the mantle wedge — the role of H2O in the genesis of mantle-derived 'arc-related' magmas: Physics of the Earth and Planetary Interiors, v. 127, no. 1–4, p. 215-232.

73. Warren, J. M., and Hauri, E. H., 2014, Pyroxenes as tracers of mantle water variations: Journal of Geophysical Research: Solid Earth, v. 119, no. 3, p. 1851-1881.

74. Xu, P., Zhao, D., 2009. Upper-mantle velocity structure beneath the North China Craton: implications for lithospheric thinning. Geophysical Journal International 177, 1279-1283.

75. Xu, Y., Tang, W., Hui, H., Rudnick, R. L., Shang, S., and Zhang, Z., 2019, Reconciling the discrepancy between the dehydration rates in mantle olivine and pyroxene during xenolith emplacement: Geochimica et Cosmochimica Acta, v. 267, p. 179-195.

76. Yuan, H. and Romanowicz, B., 2010. Lithospheric layering in the North American craton. Nature, 466(7310), pp.1063-1068.

77. Ziagos, J.P., Blackwell, D.D., Mooser, F., 1985. Heat flow in southern Mexico and the thermal effects of subduction. Journal of Geophysical Research: Solid Earth 90, 5410-5420.

CORRESPONDING AUTHOR

All correspondence and requests for materials should be addressed to Assistant Professor Emily Chin (e8chin@ucsd.edu), Scripps Institution of Oceanography, UCSD, California, USA.

AUTHOR CONTRIBUTIONS

EJC devised the study and compiled data from natural samples, and RMP performed petrological calculations. Both authors interpreted the results and wrote the manuscript.

COMPETING INTERESTS

The authors declare no competing interests.